Demantoid Garnet from Antetezambato, Northern Madagascar—Internal Characteristics and Their Use in Deciphering Geographic Origin

J. C. (Hanco) Zwaan

ABSTRACT: Demantoid garnets from Antetezambato, northern Madagascar, contain a characteristic inclusion suite typical of a skarn occurrence. Unlike demantoid from the classic deposits in the Ural Mountains, Russia, and from other serpentinite-related occurrences, the stones from Madagascar do not contain 'horsetail' inclusions, but instead host groups of small, rounded diopside grains, fluorapatite, dolomite, calcite, quartz, pyrite and wollastonite, as well as rare native bismuth. Partially healed fissures contain two-phase fluid inclusions (with H_2O and a gas bubble) of varying salinity. Negative crystals, commonly large and empty, sometimes also contain H_2O. Pronounced growth features and parallel hollow tubes are also present. Demantoid from Namibia likewise has a skarn origin and shows some similar internal features, as well as some that are different, such as the common presence of fluorapatite and small multiphase fluid inclusions, along with the absence of large negative crystals and native bismuth. A review of previously advocated methods for geographic origin determination of demantoid based on chemical fingerprinting alone shows that this technique is applicable only to stones with a nearly pure andradite composition when differentiating Malagasy and Namibian localities. In such cases, elevated traces of Mn are indicative of a Namibian origin.

In 2009, fine specimens and attractive faceted gemstones of green demantoid (as well as brown andradite) entered the market from a skarn deposit near Antetezambato in northern Madagascar (Rondeau *et al.* 2009; Pezzotta 2010; Pezzotta *et al.* 2011). The area was worked by artisanal miners until 2011 when production declined as the near-surface part of the deposit was exhausted. In 2013–2014, initial opencast mining was done by a joint venture between the Malagasy company Ruby Red Madagascar (owner of the mining rights) and a local gem-trading company.

In 2018, a new mining project was initiated by a joint venture between Ruby Red Madagascar and Prosperity Earth LLC, with mechanised equipment used to explore the deposit to a depth of 15–18 m (Gomelsky & Bates 2021). Mining is ongoing, and the company takes great pride in working in an ethical and responsible way with the local community—such as employing an all-Malagasy workforce and contributing to various initiatives pertaining to health, education, infrastructure and agriculture. The environmental footprint of the mining is also carefully considered, mainly through the replanting

Figure 1: These faceted samples of demantoid from Antetezambato, Madagascar, were selected to characterise their inclusions, with the possibility of identifying criteria for origin determination. Shown here are 19 stones (0.43–0.89 ct) of the 62 Madagascar samples in the study collection. Photo by J. C. Zwaan.
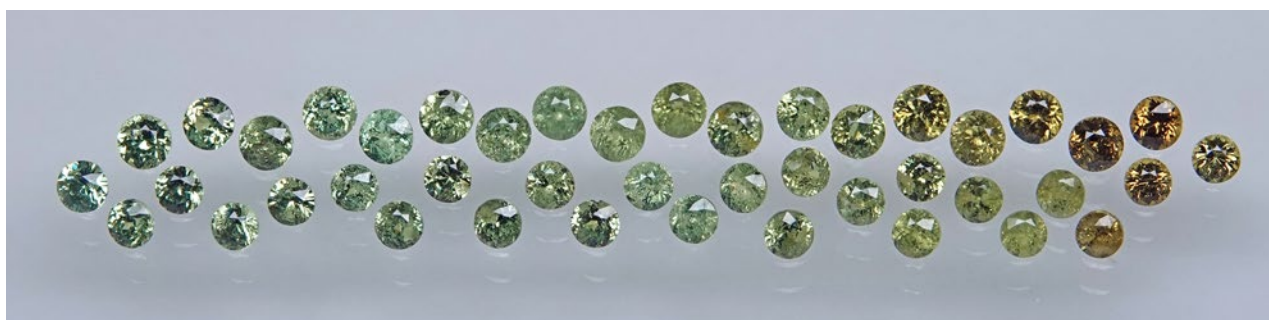
of mangroves in the area (Gomelsky & Bates 2021; J. Ferry, pers. comm. 2021).

In recent years, there has been increasing interest in the geographic origin determination of demantoid, with research focusing mainly on chemical analyses and chemometric methods (Schwarzinger 2019; Bindereif *et al.* 2020), but also on inclusion characteristics (Lewis 2018). The present study provides new data on the inclusion characteristics of demantoid from Madagascar (Figures 1 and 2), with the goal of refining criteria for origin determination. In addition, the internal microscopic features are compared to those seen in Namibian demantoid, which has a similar skarn origin. Finally, published chemical data for stones from these two deposits is evaluated further to assess the usefulness of trace-element content for aiding in their separation.

MATERIALS AND METHODS

For this study, 62 faceted Madagascar demantoids (six round brilliants and 56 round modified brilliants) ranging from 0.18 to 0.89 ct were examined (again, see Figures 1 and 2). They were loaned by Prosperity Earth LLC, and because they were selected for the presence of inclusions, these study samples are not representative of the highest-quality gem material from this locality. They were basically all transparent, moderately to heavily included (only one stone was slightly included), and some contained large fissures or cavities (or both). They varied from green to orangey yellow. Observation face-up with the unaided eye and a standard daylight-equivalent lamp showed evenly distributed colouration that ranged from an almost pure green (slightly yellowish green) to yellow-green (Munsell 10GY, 7.5GY, 5GY and 2.5GY) to greenish yellow and yellow (10Y, 7.5Y and 5Y) and, in one stone, orangey yellow (between 2.5Y and 10YR). Most colours showed light to moderate tones and were moderately saturated; the yellower stones typically appeared brownish. While samples showing a dominant green colour are classified as demantoid, the others are simply called andradite (or the trade name *topazolite*). However, boundaries between these varieties are not well

Figure 2: The remaining 43 garnets (0.18–0.36 ct) in the study collection are arranged in this photo to display the range of colour observed in the Madagascar material. Photo by J. C. Zwaan.
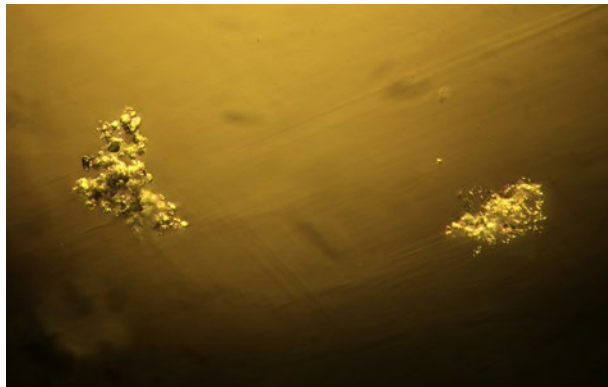
established, and they are not differentiated in this study. Overall the gems had a lively appearance, consistent with the optical properties of demantoid, which has a high (sub-adamantine) lustre and very high dispersion.

For comparison, internal characteristics were also examined in a selection of demantoid samples from the Erongo region, Namibia, showing a similar appearance. They consisted of 15 faceted stones (0.26–3.21 ct) and 23 transparent fragments (mostly with parallel polished windows; 0.79–26.24 ct). The majority of them were kindly loaned by the German-based company Paul Wild OHG, while one faceted stone and six fragments were from the Naturalis collection in Leiden, The Netherlands.

Internal features were observed with a standard gemmological microscope and a Nikon Eclipse E600 POL polarising microscope. For photomicrography, both were connected to a Nikon DS-Ri2 digital camera. Inclusions in 44 of the stones from Madagascar and 20 samples from Namibia were analysed by Raman spectroscopy using a Thermo Scientific DXR Raman microscope with 532 nm laser excitation. Scanning electron microscopy–energy dispersive X-ray spectroscopy (SEM-EDS) analyses of inclusions in two samples from Madagascar were performed using a JEOL JSM-8480LV scanning electron microscope coupled to an Oxford Instruments Inca x-act silicon drift detector (range of elements analysed: from B to U). Measurements were taken at 15 kV, with a 40 s acquisition time for each analysis and a 3 µm spot size.
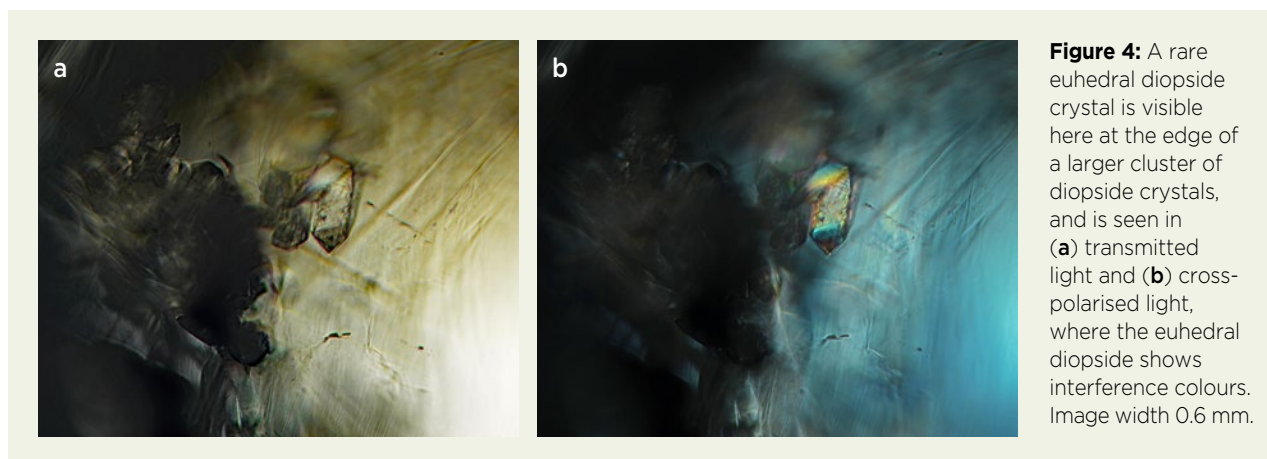
MICROSCOPIC CHARACTERISTICS

The internal features described in this section all pertain to the Madagascar samples, while those observed in the demantoids from Namibia are compared further below in the Discussion section. All of the photomicrographs were taken by the author.
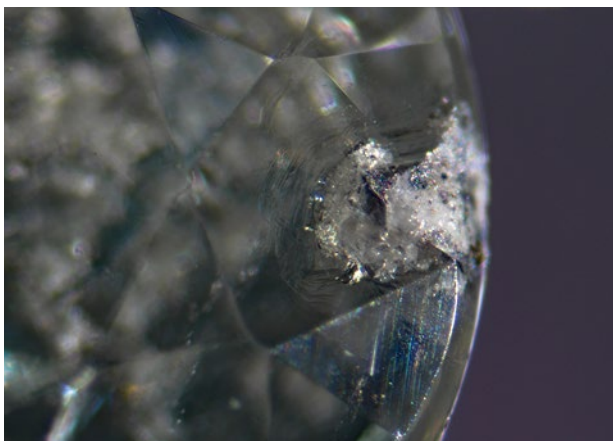

Figure 3: Clusters of small diopside crystals were encountered in most of the demantoids studied. The cluster on the right especially displays a 'bread-crumb' appearance due to the minute size of most of the individual crystals. Oblique illumination; image width 0.63 mm.

Mineral Inclusions

The most commonly encountered mineral inclusion (confirmed in 37 of the 44 samples analysed by Raman spectroscopy) was diopside, which occurred as small, mostly rounded, equidimensional grains that were grouped in clusters. Individual stones contained from one to many such clusters. When viewed with a loupe or with low magnification, the clusters looked like 'bread crumb' inclusions. At higher magnification, it became apparent that most of the individual diopside grains were very small and rounded (Figure 3). Occasionally, slightly larger grains and, rarely, euhedral crystals of diopside were present (Figure 4). Many of the clusters were analysed with Raman spectroscopy to see whether any other minerals were present, but none were found. Raman analysis gave the best match to clinopyroxene, and in particular to diopside. The positions of the Raman peaks and their comparatively low full-width-at-half-maximum values indicated a relatively pure diopside composition ($CaMgSi_2O_6$), compared to various

Figure 4: A rare euhedral diopside crystal is visible here at the edge of a larger cluster of diopside crystals, and is seen in (**a**) transmitted light and (**b**) cross-polarised light, where the euhedral diopside shows interference colours. Image width 0.6 mm.

Figure 5: Carbonate inclusions in demantoid from Madagascar include whitish aggregates of dolomite. Image width 2.0 mm.
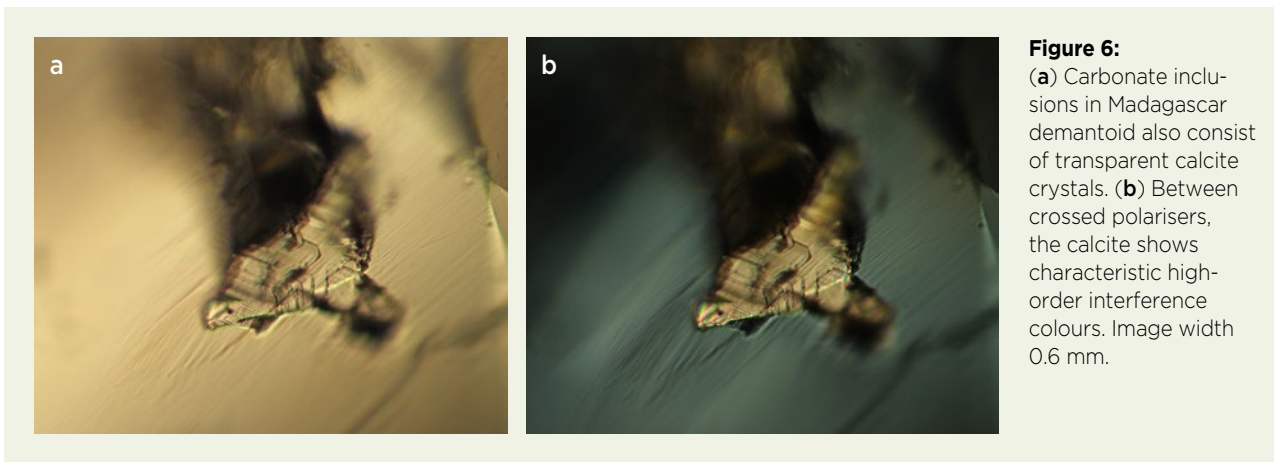
diopside-clinoenstatite mixtures ($CaMgSi_2O_6$–$Mg_2Si_2O_6$; cf. Tribaudino *et al.* 2012). An increase in Fe concentration—as expected for hedenbergite ($CaFeSi_2O_6$) and augite ($[Ca,Mg,Fe^{2+}]_2Si_2O_6$) components—would shift most Raman bands to lower wavenumbers (cf. Huang *et al.* 2000; Buzatu & Buzgar 2010). A semi-quantitative

SEM-EDS analysis of a diopside inclusion at the surface of one demantoid sample confirmed its nearly pure composition (in wt.%): MgO 17.0, SiO_2 57.2, CaO 24.4 and FeO 1.35, giving $Ca_{50.0}Mg_{47.8}Fe_{2.2}$ (or X_{Mg} = 0.96).
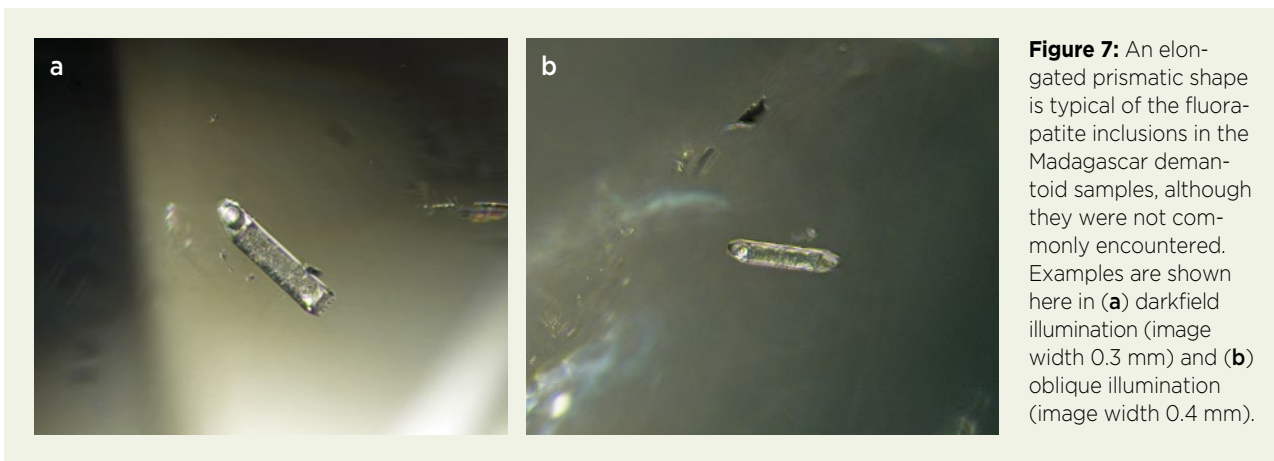
Carbonate inclusions were confirmed in nine of the demantoids. They occurred as whitish aggregates of small grains (Figure 5) and as small, transparent crystals, some with a rhombohedral shape (Figure 6). Raman spectroscopy revealed that the whitish aggregates consisted of dolomite ($CaMg[CO_3]_2$) and the transparent crystals were calcite ($CaCO_3$).

Small, transparent apatite crystals were occasionally identified. They were mostly prismatic (Figure 7), although one rounded apatite grain was also found. Raman spectroscopy gave a best match with fluorapatite ($Ca_5[PO_4]_3F$) in the RRUFF database (https://rruff.info).
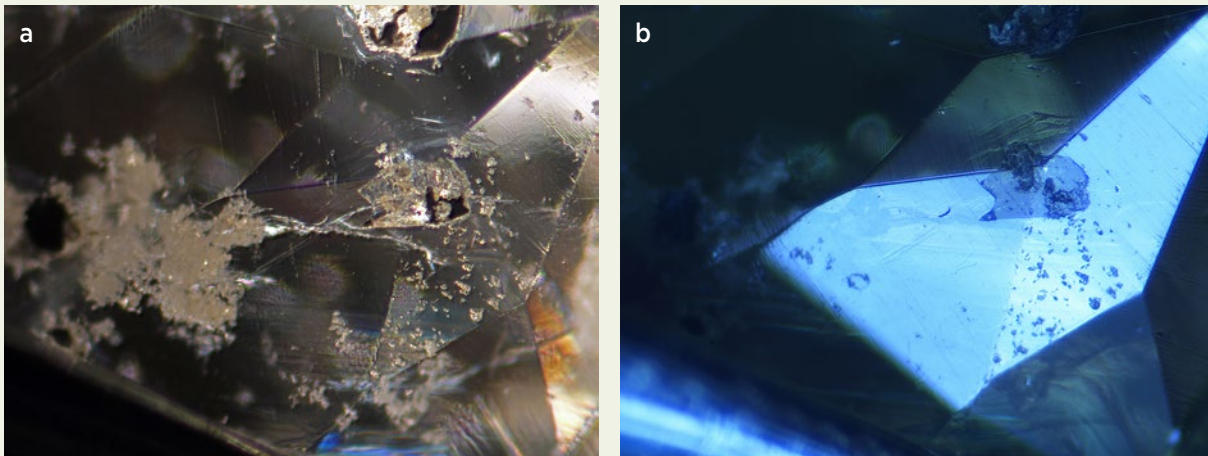
Quartz was not commonly observed, but it might have just been elusive, occurring as colourless grains in proximity to the many clusters of diopside and other inclusions. One quartz grain was spotted at the surface of a sample by its much lower lustre compared with the demantoid host (Figure 8). Another quartz inclusion
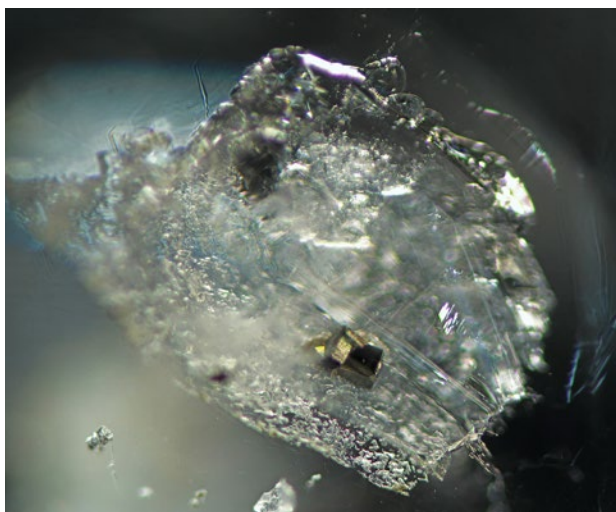

Figure 6: (**a**) Carbonate inclusions in Madagascar demantoid also consist of transparent calcite crystals. (**b**) Between crossed polarisers, the calcite shows characteristic high-order interference colours. Image width 0.6 mm.

Figure 7: An elongated prismatic shape is typical of the fluorapatite inclusions in the Madagascar demantoid samples, although they were not commonly encountered. Examples are shown here in (**a**) darkfield illumination (image width 0.3 mm) and (**b**) oblique illumination (image width 0.4 mm).

Figure 8: Quartz inclusions were rarely identified in the Madagascar demantoid samples. (**a**) A quartz inclusion is located near a cluster of diopside crystals in a rather heavily included stone, seen here in darkfield illumination. (**b**) Its presence is betrayed by a significantly lower lustre than the host demantoid where it intersects the surface when viewed with reflected light. Image width 1.6 mm.
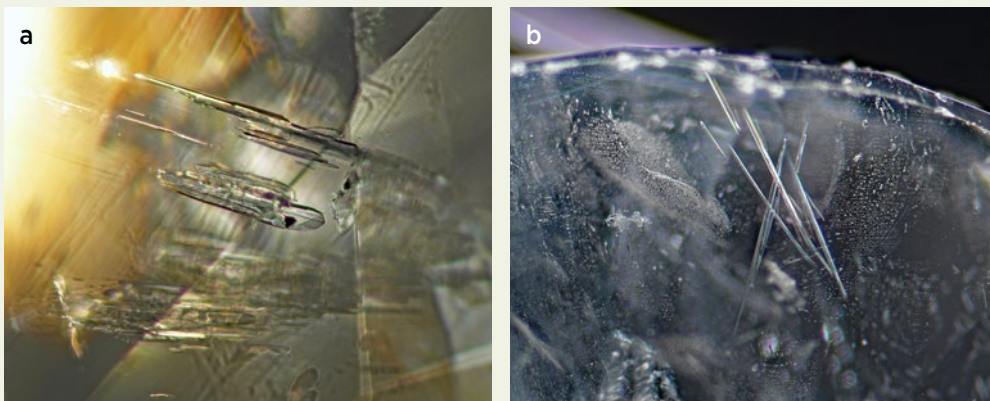

Figure 9: In this Madagascar demantoid, a transparent quartz inclusion is present above a partially healed fissure and hosts interpenetrant pyrite cubes. Darkfield and oblique illumination; image width 1.2 mm.

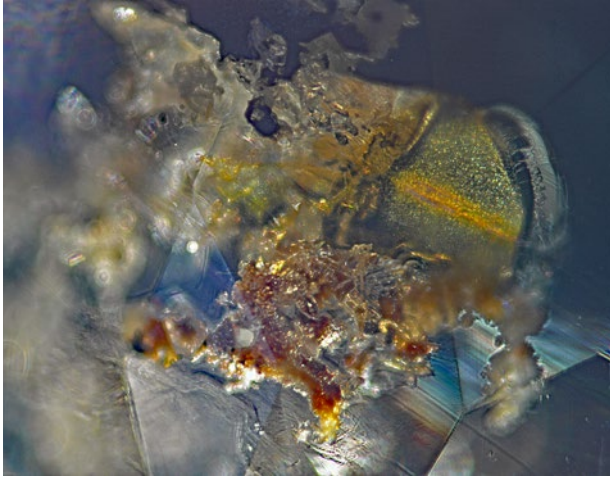was positioned above a partially healed fissure and contained interpenetrant pyrite cubes (Figure 9).

Wollastonite ($CaSiO_3$) was identified in two of the stones. It occurred as transparent, long prismatic to needle-like crystals (Figure 10). Very small wollastonite inclusions varied from elongate to more equidimensional and slightly rounded. Although the Raman spectra obtained were mixed with the signals of the host demantoid, wollastonite could readily be identified, matching well with reference spectra in the RRUFF database.

Several of the studied demantoids contained iron-stained fissures (Figure 11), which were typically small. In one stone, Raman analysis confirmed the presence of goethite.

Notably, three of the stones contained opaque needle- or rod-like inclusions with a metallic lustre (Figure 12). Two of these inclusions were parallel-oriented, and Raman analysis where they intersected the surface revealed a
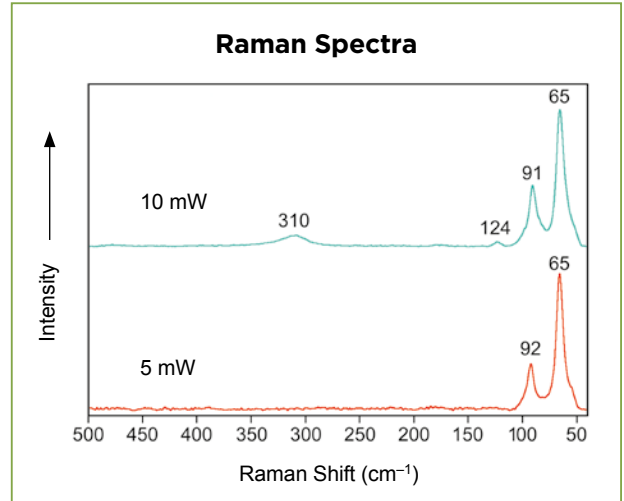

Figure 10:
(**a**) Long prismatic crystals and (**b**) needles of wollastonite are rarely present in Madagascar demantoid. (a) Transmitted light, image width 1.1 mm; and (b) darkfield illumination, image width 1.8 mm.

Figure 11: In this Madagascar demantoid, goethite is present in a relatively large fissure, appearing as small orangey brown flakes and brownish yellow microcrystals. Darkfield illumination, image width 2.5 mm.

Figure 13: The Raman spectrum of a surface-reaching bismuth inclusion analysed with 10 mW excitation shows weak features at 310 and 124 cm⁻¹, which indicate the presence of bismite, as expected for the oxidation of bismuth. These features are not visible in the spectrum obtained with 5 mW excitation, consistent with the oxidation process being hastened by higher laser power.

spectrum (in the low-wavenumber range) characteristic of native bismuth, with a strong band at about 65 cm^{-1} and another pronounced feature at about 91 cm^{-1} (Chukanov & Vigasina 2020). Native bismuth is easily oxidised in air and can alter to bismite (Bi_2O_3), and this may be hastened by increasing the laser power during Raman analysis (Zepeda *et al.* 2012). After raising the laser power from 5 to 10 mW, relatively weak, broad features appeared at 310 and 124 cm^{-1}, indicating the presence of ß-Bi_2O_3 (Figure 13). SEM-EDS analysis confirmed the presence of Bi along with varying small amounts of oxygen. Ten analyses (four on one bismuth inclusion and six on another) gave Bi = 91.1–95.2 wt.% and O = 4.8–8.9 wt.%.

In one other demantoid, Raman analysis again confirmed the presence of native bismuth. This inclusion was a bit thicker and appeared bent and branch-like (Figure 14a). Its characteristic silvery grey-white colour
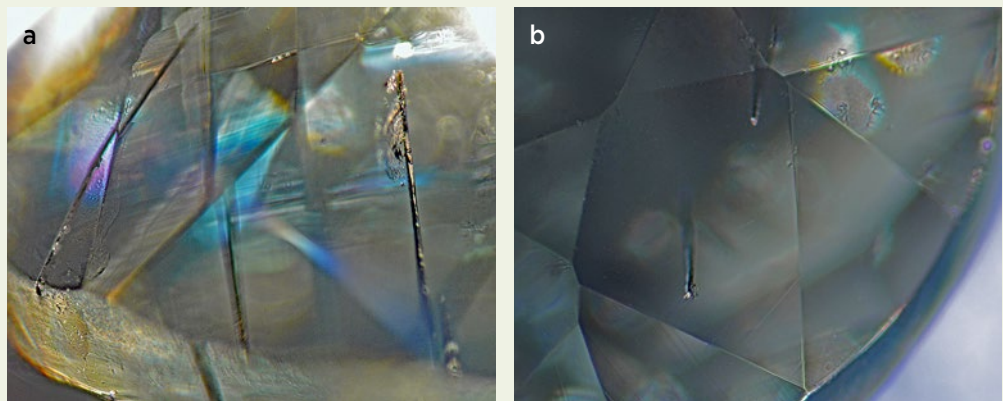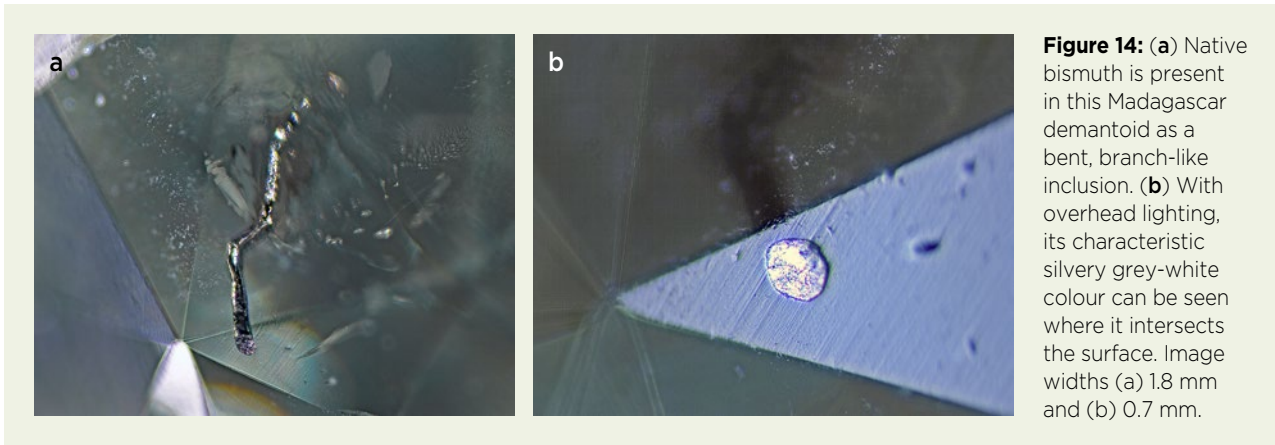
and high lustre were apparent where it intersected the surface (Figure 14b).

In another demantoid, irregular grains were encountered that looked like an ore mineral and were associated with a partially healed fissure (liquid feather). The grains appeared steel-grey to black, with an olive green overtone (Figure 15). Raman spectroscopy suggested the presence of stannite (Cu_2FeSnS_4), which is consistent with the visual appearance of the grains. Because the inclusions were small and relatively deep under the surface, the resulting Raman spectra were mixed with strong bands of the host demantoid. Nevertheless, after multi-component analysis of a representative mixed spectrum, the strongest band generated by the inclusion had a peak

Figure 12: Opaque, needle-like inclusions with a metallic lustre in Madagascar demantoid are shown with (**a**) oblique illumination and (**b**) darkfield illumination. Raman analysis identified them as native bismuth. Image width 1.7 mm.

Figure 14: (**a**) Native bismuth is present in this Madagascar demantoid as a bent, branch-like inclusion. (**b**) With overhead lighting, its characteristic silvery grey-white colour can be seen where it intersects the surface. Image widths (a) 1.8 mm and (b) 0.7 mm.
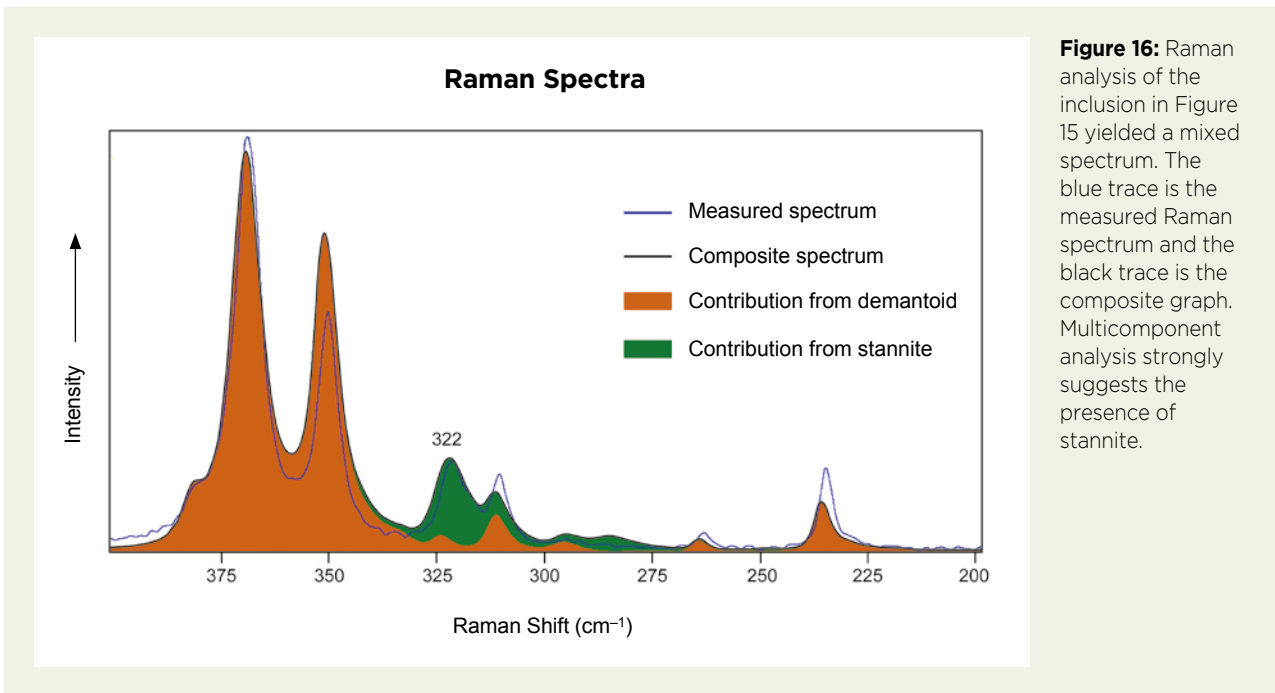

Figure 15: In one Madagascar demantoid, irregular metallic grey-to-black grains (probably stannite) are associated with a partially healed fissure. Image width 0.8 mm.

position of 322 cm⁻¹ (Figure 16), which exactly matches with the principal peak of the stannite spectra in the RRUFF database.
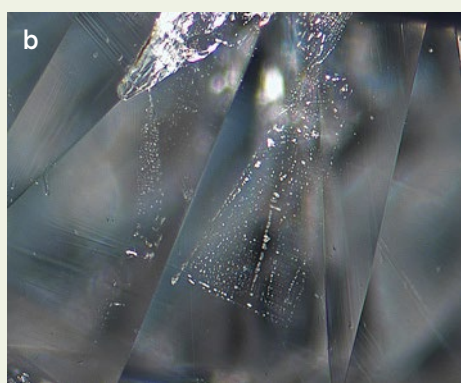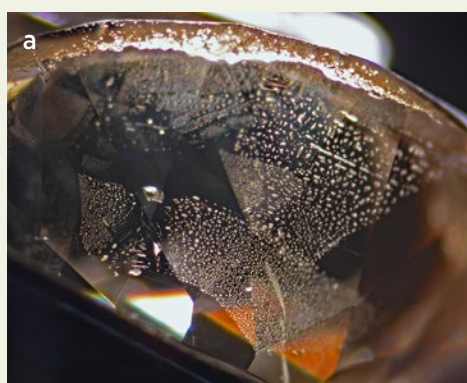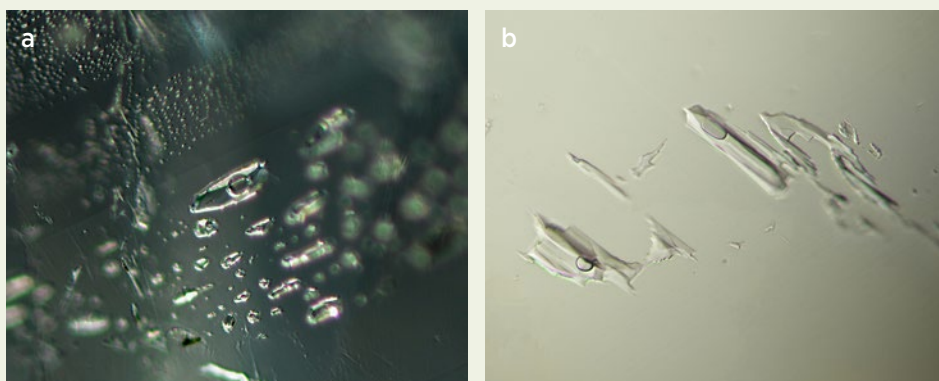
Fluid Inclusions

Partially healed fissures were common, taking on various forms. Some contained clearly discernible two-phase inclusions with regular shapes, often elongated or rounded (or both; Figure 17a), but also with slightly jagged or irregular forms (Figure 17b) that were similar to those of 'trichites' in tourmaline. Other partially healed fissures were more veil-like, containing minute voids, and were fairly large or showed a characteristic triangular ('pine tree') shape (Figure 18).

Raman analysis confirmed that the two-phase inclusions consisted of aqueous liquid-vapour phases. Spectra
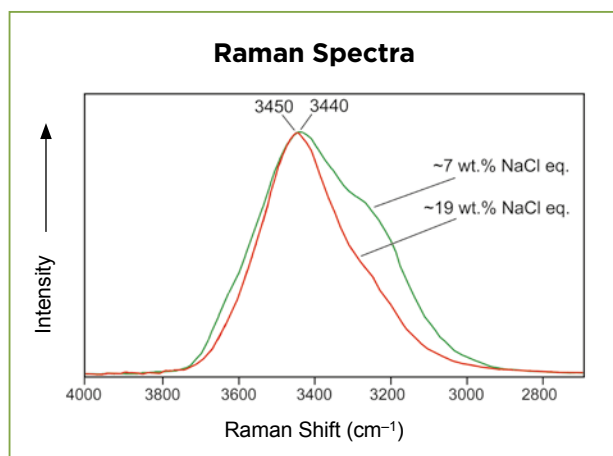

Figure 16: Raman analysis of the inclusion in Figure 15 yielded a mixed spectrum. The blue trace is the measured Raman spectrum and the black trace is the composite graph. Multicomponent analysis strongly suggests the presence of stannite.

Figure 17: Partially healed fissures in Madagascar demantoid often contain clearly discernible two-phase inclusions, both as (**a**) elongated, rounded shapes and as (**b**) jagged or irregular forms. (a) Darkfield illumination, image width 0.4 mm; and (b) transmitted light, image width 0.3 mm.

Figure 18: (**a**) Large, veil-like, partially healed fissures are common in Madagascar demantoid. (**b**) These fissures frequently occur in triangular shapes reminiscent of pine trees. Darkfield illumination, image widths (a) 2.3 mm and (b) 1.4 mm.

of both types of inclusions (elongated, rounded shapes and trichite-like ones) showed a typical O-H stretching band of liquid water. In general, Raman features at 3430 and 3232 cm^{-1} can be regarded as the most distinctive components of pure water (Sun 2010). However, the overall position and shape of the O-H stretching band depend on both the temperature at which they are analysed and the NaCl concentration in the fluid.
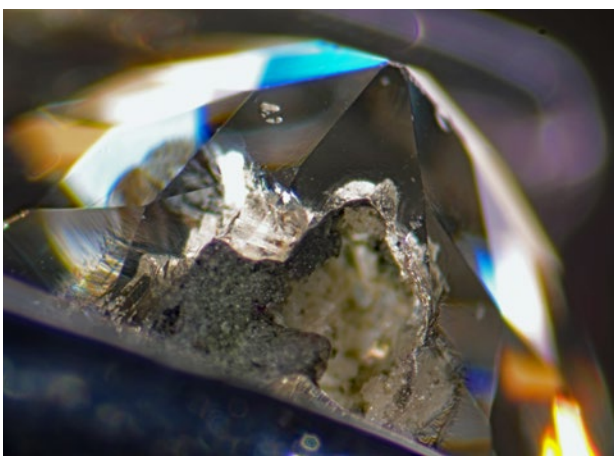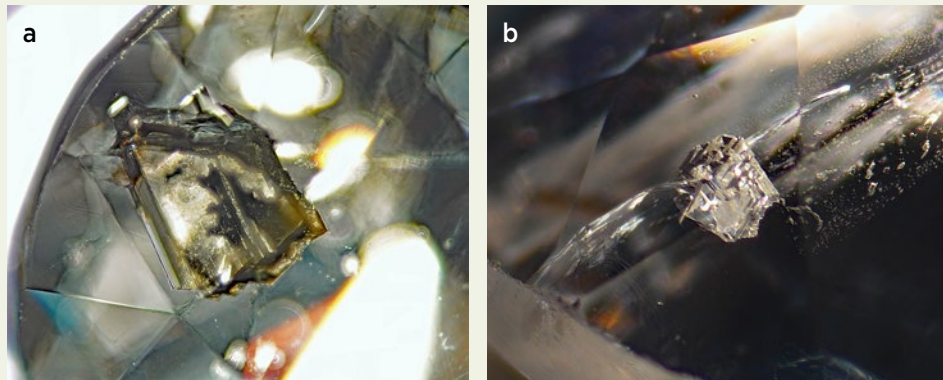
Measurements were done at a fixed room temperature of 20ºC. At this temperature, as the NaCl concentration increases, the position of the O-H stretching band shifts to higher wavenumbers—in this case to 3440 and 3450 cm^{-1}, corresponding to lower and higher salinity, respectively—while the shoulder of this band diminishes and its slope steepens (see Figure 19). On this basis, using signal processing and equations given by Claverie *et al.* (2010), the rounded-shaped inclusions likely contain about 70 g/L NaCl and the trichite-like ones have up to about 190 g/L NaCl, which translates to salinities of 7 wt.% and 19 wt.% NaCl equivalent. Although the latter value is relatively high, it is not elevated enough to produce three-phase inclusions with halite cubes upon cooling, such as those seen in Colombian emeralds (Bodnar 2003).
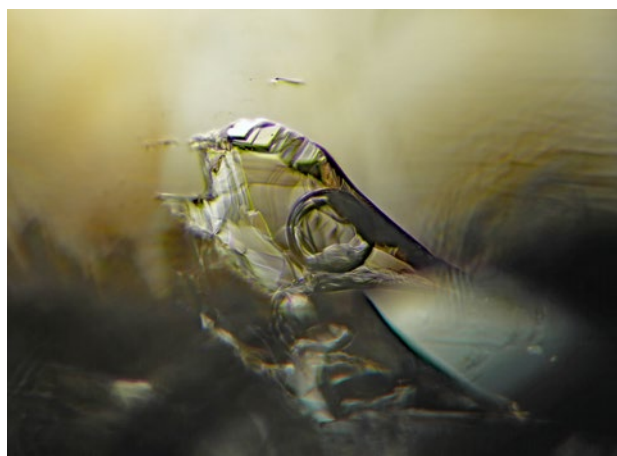

Figure 19: Raman spectra of the aqueous liquid-vapour inclusions in Figure 17a (green trace) and 17b (red trace) show an O-H stretching band of liquid water. The shape and position of the band indicate that these aqueous inclusions contain different concentrations of NaCl, which reduces the strength of the shoulder at around 3200–3300 cm^{-1} as salinity increases.

Figure 20: Negative crystals are common in Madagascar demantoid. In the study samples shown here, they exhibit (**a**) large size and (**b**) rhombohedral shape. Image widths (a) 1.2 mm and (b) 1.4 mm.
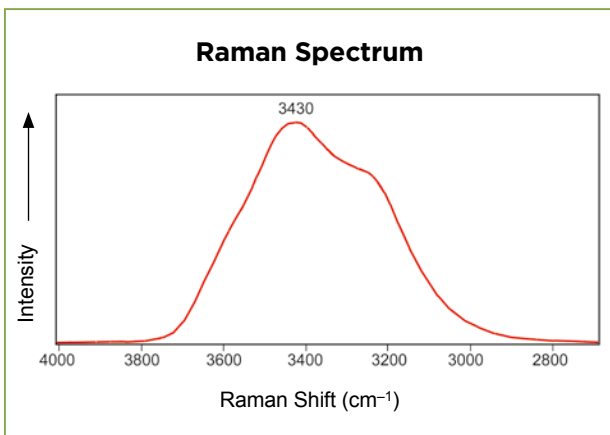

Figure 21: A large negative crystal on the pavilion of this Madagascar demantoid has collected some debris where it is open to the surface. Image width 2.5 mm.

Figure 22: Negative crystals in Madagascar demantoid are mostly empty, but occasionally contain water (liquid and vapour), as seen in this example. Image width 0.9 mm.

Negative Crystals

Inclusions showing high relief and having the appearance of crystals were also very common (Figure 20a). When analysed with Raman spectroscopy, these 'crystals' mostly turned out to be empty, which identifies them as

Raman Spectrum

3430

Intensity

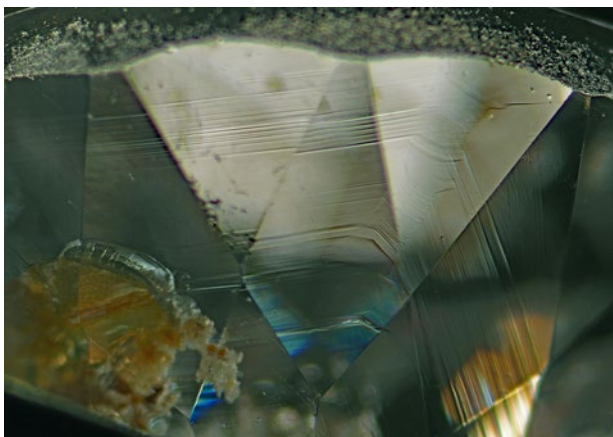4000 3800 3600 3400 3200 3000 2800

Raman Shift (cm⁻¹)

Figure 23: The Raman spectrum of the negative crystal in Figure 22 indicates the presence of relatively pure water when compared to the spectra in Figure 19 of the saline inclusions.

negative crystals. Many showed rhombohedral shapes (Figure 20b). Several large negative crystals intersected the surface of one faceted stone, creating a large empty cavity that was partially filled with foreign material (probably dirt and remnants of polishing powder; Figure 21). Occasionally, the negative crystals were found to contain a fluid and gas bubble (Figure 22). The ones that could be analysed showed a Raman spectrum of pure water (Figure 23), rather than the saline-type spectra of the fluid inclusions constituting the partially healed fissures (cf. Figure 19). However, establishing whether these trends for the water-containing inclusions are consistent would require many more measurements and a more detailed fluid inclusion study.

Growth Structures and Growth Tubes

Straight and angular growth zoning were observed in a number of stones. While the colour was usually even, the zoning had a similar appearance to the so-called graining observed in diamond: very narrowly spaced zones, with occasionally brown and reflective graining
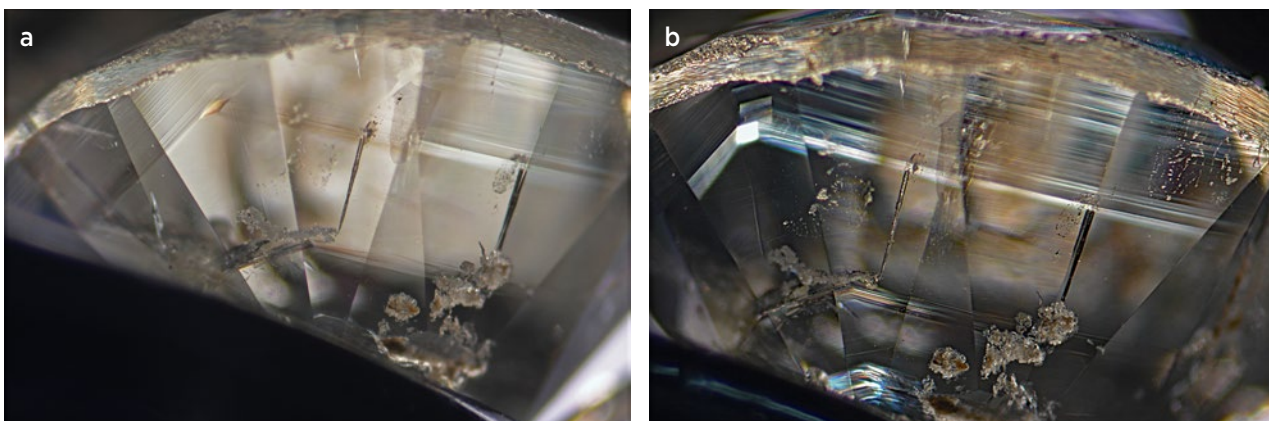
Figure 24: Straight and angular growth zoning observed in Madagascar demantoid sometimes resembles the narrow-spaced graining in diamonds. Image width 2.2 mm.

(Figures 24 and 25). Tube-like inclusions were oriented perpendicular to straight growth zoning. Some larger inclusions of this kind that reached the surface could be confirmed as hollow tubes (Figure 26a). Also perpendicular to the graining were minute, parallel-oriented, short needle-like inclusions (Figure 26b), as well as minute

particles that remain undetermined. Unusual stepped growth zoning was found in one stone (Figure 27).
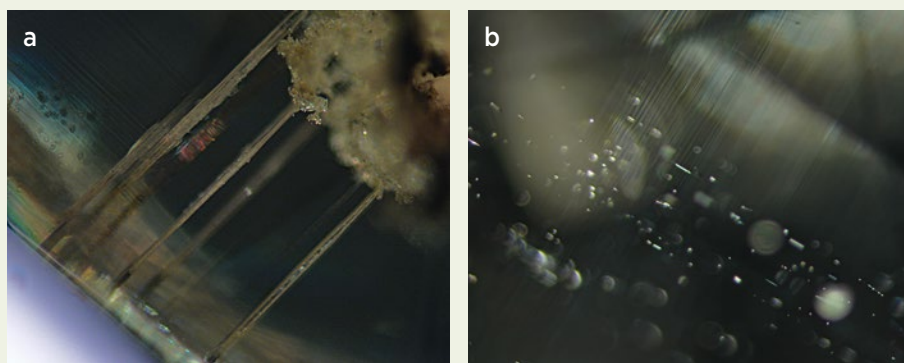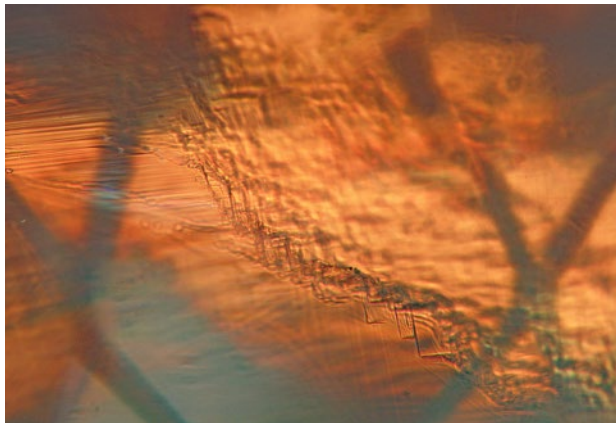
DISCUSSION

The assemblage of mineral inclusions in the Madagascar study samples—in particular diopside, wollastonite, calcite, dolomite and quartz—is consistent with the formation of this demantoid in a skarn environment, as described previously (Pezzotta 2010; Pezzotta *et al.* 2011). Based on these inclusions, the stones from Madagascar can readily be distinguished from demantoid of Russia, Italy, Pakistan, Iran, Eritrea and Slovakia, which is generally related to serpentinite resulting from hydrothermal/metamorphic alteration of ultramafic parent rocks. Demantoid from Russia and Italy contains radially arranged and curved fibres of asbestos (i.e. chrysotile, as so-called horsetail inclusions) and chromite grains (Gübelin & Koivula 2005; Adamo *et al.* 2009; Lewis 2018). Horsetail inclusions are also common in demantoid from Pakistan (i.e. Baluchistan; Adamo *et al.* 2015), Iran (Gübelin & Koivula 2005; Du Toit *et al.* 2006), Eritrea (Milisenda & Hunziker 1999) and

Figure 25: Occasionally, depending on the lighting direction, areas of brown graining (**a**) are seen as striking reflective graining (**b**) in Madagascar demantoid. Also visible are parallel tubes that are oriented perpendicular to the growth zoning. Near the bottom of each image, clusters of diopside are present. Image widths (a) 3.0 mm and (b) 2.6 mm.

Figure 26: (**a**) Larger tubes oriented perpendicular to the growth zoning reach the surface of this Madagascar demantoid sample, allowing verification that they are indeed hollow. (**b**) Short, very fine needles, also perpendicular to the growth zoning, are occasionally present in Madagascar demantoid. Image width 1.2 mm for both.

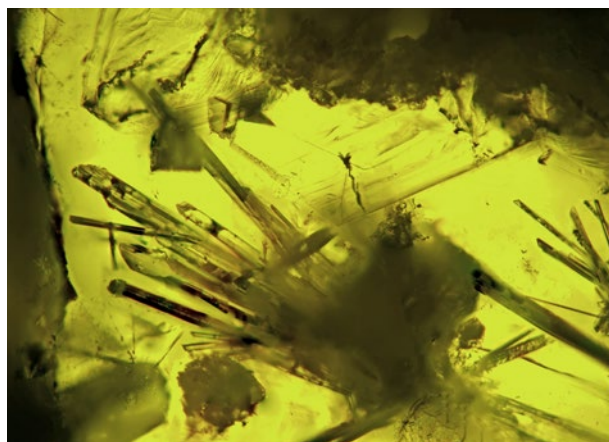**Figure 27:** Unusual stepped growth zoning is visible in this Madagascar demantoid. Image width 1.0 mm.

Slovakia (Štubňa *et al.* 2019). In addition, demantoid from Italy and Baluchistan commonly contains white masses of a serpentine mineral, probably antigorite. Demantoid from Baluchistan also hosts equant octahedral (Cr-rich) magnetite which, together with the serpentine, resembles the chromite + serpentine assemblage in demantoid from Italy (Adamo *et al.* 2009, 2015; Palke & Pardieu 2014).

Demantoid found in the peridot mines within the Pakistan part of Kashmir (northern Pakistan) shows acicular, fibrous and felt-like chrysotile, but which is not radially arranged, as in demantoid from Russia (Milisenda *et al.* 2001). Only the partially healed fissures in demantoid from northern Pakistan and Iran (Milisenda *et al.* 2001; Du Toit *et al.* 2006) sometimes look similar to those encountered in this study. The equidimensional, rounded, small diopside crystals that occur in clusters in our study samples are very different from the stalk-like diopside inclusions that are sometimes present in demantoid from the Ural Mountains (Krzemnicki 1999; Gübelin & Koivula 2005).
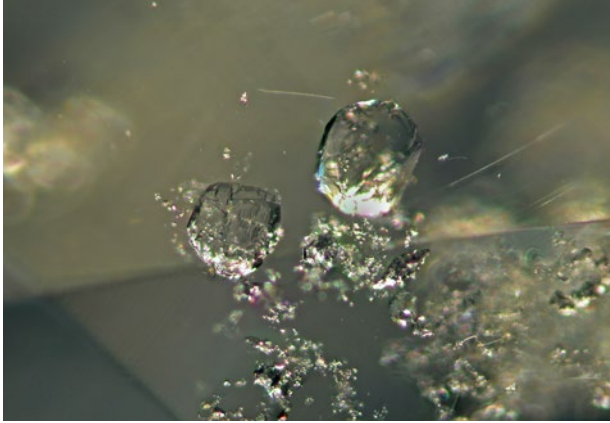
The inclusions in demantoid from Madagascar are most similar to those in the stones from Namibia, which also formed in a skarn environment. It has been reported previously that Namibian demantoid contains diopside (X_{Mg} = 0.92–0.95), wollastonite, quartz, calcite and sphalerite, and it also shows similar growth zoning (Lind *et al.* 1998; Koller *et al.* 2012; Lewis 2018). Furthermore, Koller *et al.* (2012) stated that the fluid inclusions (two-phase and multiphase) in Namibian demantoid have a secondary origin, because the fluids were trapped along partially healed fractures. Based on micro-thermometric measurements, Koller *et al.* (2012) and Giuliani *et al.* (2017) suggested that the fluid inclusions in Namibian demantoid belong to the H_2O-$CaCl_2$ system (with or without CH_4), with the liquid phase having a salinity of 6–8 wt.% $CaCl_2$ and with CH_4 present in the vapour phase.

From the present author's observations of the 38 comparison samples from Namibia, at first glance they showed a similar inclusion scenery to Madagascar demantoid. Both contained diopside clusters and the common presence of partially healed fissures, as well as reflective, straight and angular growth zoning. Also seen in the Namibian demantoid were wollastonite (in three samples), a transparent calcite rhombohedron and small quartz grains.

However, closer examination revealed some notable differences. Raman analyses of a number of long prismatic and small, almost needle-like crystals in Namibian demantoid—with the same appearance as the wollastonite in the three other Namibian stones mentioned above—gave spectra of quartz or a mixture of calcite and quartz (suggesting calcite-quartz pseudomorphs after wollastonite; Figure 28). Also, fluorapatite was a common inclusion in Namibian demantoid, often occurring adjacent to or within the clusters of small diopside crystals, whereas fluorapatite was only occasionally encountered in the Madagascar samples. In Namibian demantoid, rounded, transparent grains of fluorapatite were more common and significantly larger than the long prismatic crystals present in the Madagascar stones. The largest of the few fluorapatite crystals encountered in the Madagascar demantoid were approximately 100-µm-long prisms (Figure 7b), while in the Namibian material equidimensional, rounded crystals up to approximately 200 µm were common (Figure 29). Sphalerite was reported previously in Namibian demantoid but was not found in this study. Titanite was identified (with Raman analysis) as a rare inclusion adjacent to a large cluster of diopside grains in a Namibian sample.

Figure 28: Long prismatic crystals of wollastonite occur in demantoid from Namibia. Interestingly, Raman analysis of the elongate inclusions shown here yielded quartz spectra, suggesting the presence of quartz pseudomorphs after wollastonite. Image width 1.4 mm.
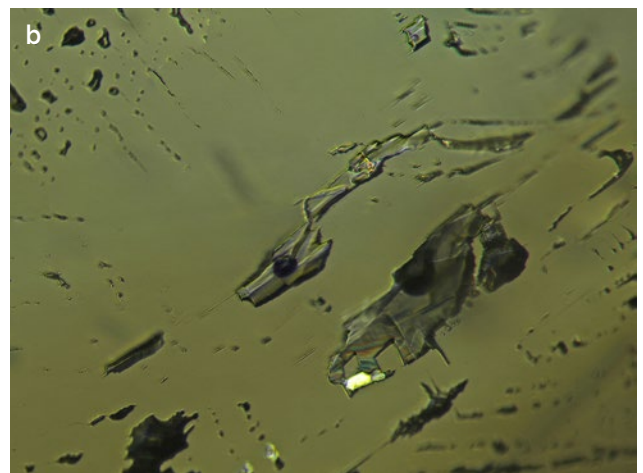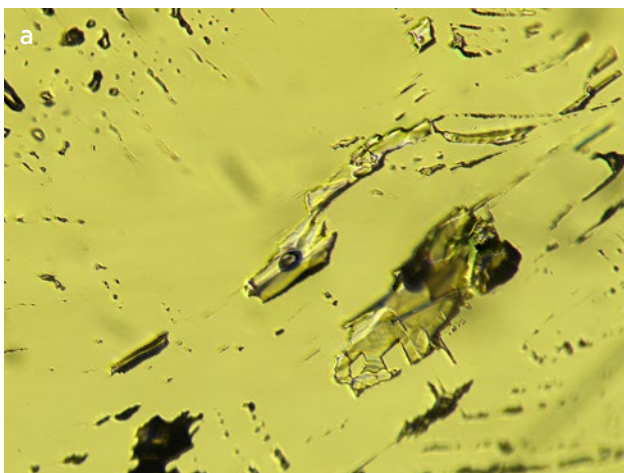
Figure 29: The transparent, rounded fluorapatite inclusions observed in Namibian demantoid are both much more common and somewhat larger than those occasionally seen in Madagascar material. Image width 0.9 mm.

Partially healed fissures in the Namibian demantoid samples were typically veil-like, commonly containing minute fluid inclusions, and sometimes showing trichite-like patterns, which often looked dark. Raman analysis suggested they were empty. In addition, small two-phase and multiphase fluid inclusions containing minute, doubly refractive solids were present in the Namibian stones. Some slightly larger fluid inclusions could be analysed, which revealed that they contained small grains of calcite, liquid H_2O and a gas bubble (Figure 30). This suggests the presence of Ca-bearing aqueous solutions during the formation process. Raman analysis of H_2O in some fluid inclusions did not reveal the presence of ClO_4^-, CCl_4 or $CaCl_2$, probably because, if present, their concentrations were not high enough to be detected (cf. Rudolph & Irmer 2013; Martinez-Uriarte *et al.* 2014). Either pure H_2O or water with very

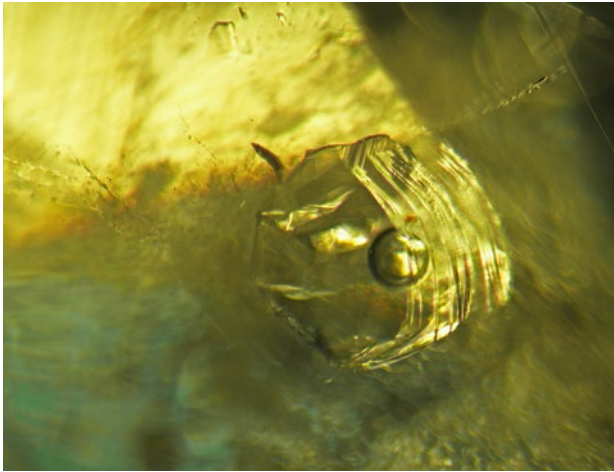low salinity (up to ~10 wt.% NaCl equivalent) was found, corresponding to 6% in the $CaCl_2$-H_2O system (after Roedder 1984). This is consistent with findings by Koller *et al.* (2012), who inferred the presence of $CaCl_2$ by the measurement of low melting points during their micro-thermometric freezing-stage experiments. As in the Madagascar material, neither CH_4 nor CO_2 could be found in the vapour phase of the fluid inclusions in Namibian demantoid. In any case, an in-depth fluid inclusion study of the demantoids and their host rocks from both Madagascar and Namibia would be required to fully characterise the fluids involved with the formation environment of the garnets.

Negative crystals were rarely seen in the Namibian demantoid, and those encountered were comparatively small. Large, empty negative crystals on the order of 600–1000 µm that were seen in the Madagascar samples (Figures 20a and 21) were not present in either the faceted stones or the polished crystal fragments from Namibia. Only one Namibian demantoid hosted a negative crystal containing water (liquid and vapour) that was similar in appearance and size (slightly larger than 400 µm) to those seen in Madagascar material (Figure 31; compare to Figure 22).

In summary, demantoid from Madagascar shows a highly characteristic inclusion scenery: a combination of diopside clusters and negative crystals (the latter being commonly large and empty, but occasionally filled with aqueous liquid and vapour), along with partially healed fissures, in combination with the absence of calcite-bearing multiphase inclusions. Bismuth rods have not been reported as an inclusion in demantoid from any other occurrence, so when present these might serve to prove a Madagascar origin.

Figure 30: (**a**) Multiphase inclusions in Namibian demantoid were found to contain water (liquid and vapour), and no CH_4 or CO_2 in the vapour phase, similar to those analysed in the Madagascar samples. (**b**) Between crossed polarisers, a birefringent calcite crystal is revealed in one of the multiphase inclusions. Image width 0.7 mm.

Figure 31: One of the Namibian demantoid samples hosts a negative crystal containing water, similar to those occasionally present in Madagascar demantoid. Image width 1.2 mm.

Evaluation of Previous Demantoid Chemical Data

Chemical data for Madagascar demantoid were initially given by Bocchio *et al.* (2010) and Pezzotta *et al.* (2011). Compared with those from serpentinised rocks, stones from Madagascar show no significant to very low Cr, V and Ti, low Mg and Mn, and high rare-earth element (REE) concentrations. Demantoid with a nearly pure andradite composition is typically enriched in light REEs, depleted in heavy REEs and shows a positive Eu anomaly (Bocchio *et al.* 2010).
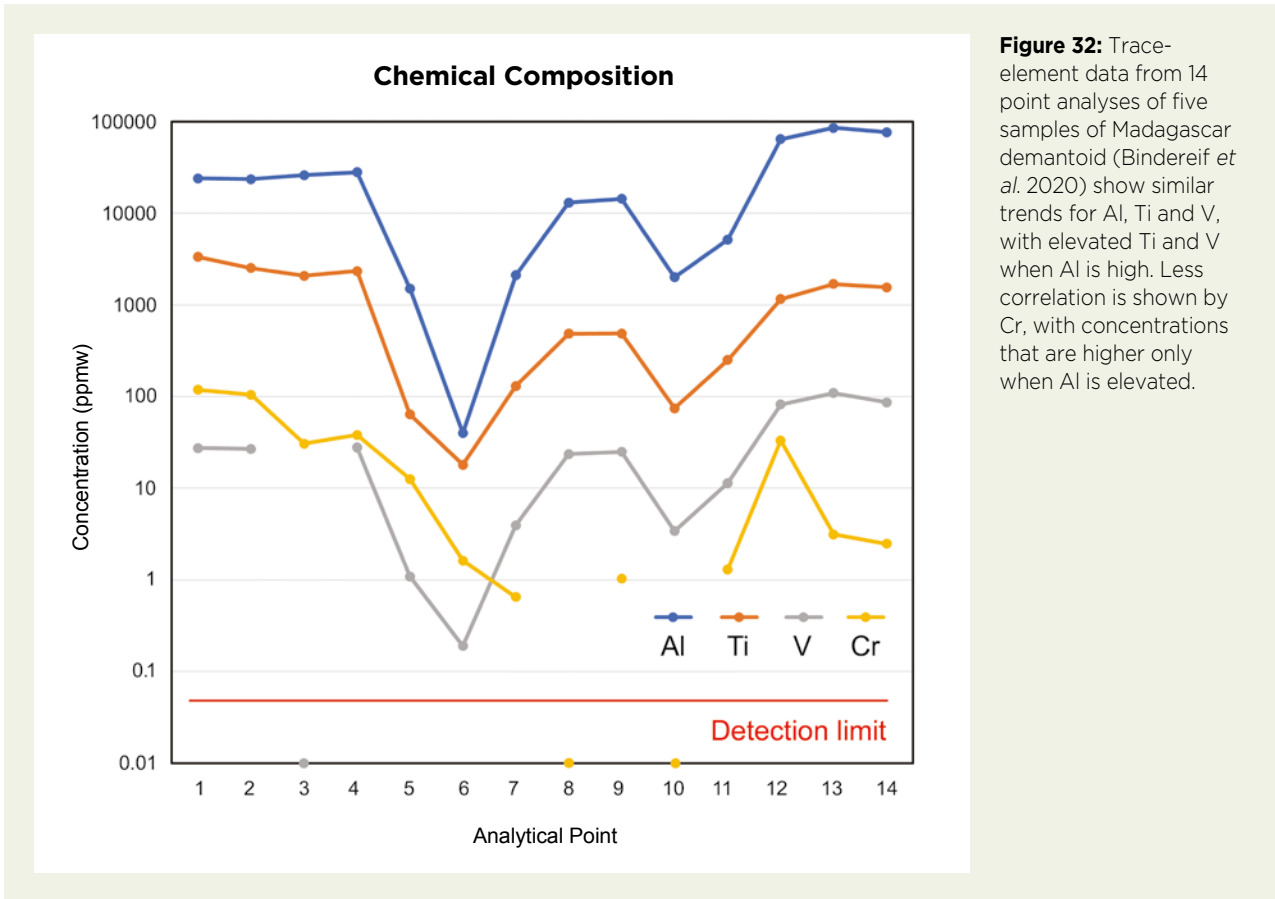
Consistent with their formation in a skarn environment, demantoids from both Madagascar and Namibia have a similar chemical composition (Bocchio *et al.* 2010; see also data in Table I). Nevertheless, Schwarzinger (2019) and Bindereif *et al.* (2020) advocated distinguishing them based on chemical fingerprinting (using Al content and plotting V+Cr vs Mn/Ti ratio) or chemometric modelling using logarithms of trace-element concentrations for Mg, Al, Ti, V, Cr and Mn. However, some of their Madagascar data show extremely high Al, much higher Ti, and significantly higher V and Cr than the data presented by Pezzotta *et al.* (2011), who gave Mg, Al, Ti, V and Cr concentrations more similar in most cases to those for Namibian material (Table I). These differences might be due to the fact that compositional variations can occur on a very local scale. While most demantoid is almost pure andradite (Adr; end-member composition $Ca_3Fe_2^{3+}[SiO_4]_3$), it may also contain a significant grossular component (Grs; end-member composition $Ca_3Al_2[SiO_4]_3$). Bocchio *et al.* (2010) analysed a single zoned sample from Namibia that varied from almost pure andradite to a composition enriched in grossular ($Adr_{11}Grs_{89}$). Barrois *et al.* (2013) mentioned that samples from Madagascar sometimes show narrow Al-rich zones, with up to 5.9 wt.% Al_2O_3 (i.e. ~31,230 ppmw Al), alternating with Al-free zones or Al-rich second-generation andradite in small cavities. Bindereif *et al.* (2020) reported Al values up to 85,470 ppmw (which converts to 16.15 wt.% Al_2O_3) in samples from Madagascar, demonstrating a significant grossular component. A plot of the 14 point analyses of five samples of Madagascar demantoid reported in Bindereif *et al.* (2020) shows that elevated Ti,

Table I: Relevant element concentrations (by LA-ICP-MS) in demantoids from Madagascar and Namibia.

Property	Madagascar			Namibia	
	Pezzotta *et al.* 2011		Bindereif *et al.* 2020*	Bindereif *et al.* 2020*	
No. samples	13		5	25	
No. analyses	150		14	73	
Element (ppmw)	Range	Median	Range	Range	Median
Mg	307–1423	450	171–776	70–1145	321
Al	15–5467	38	40–85470	13–981	117
Ti	0.17–7.5	1.2	18–3325	0.63–98	4.4
V	nd–3.1	0.03	nd–109	nd–7.3	0.24
Cr	nd–2.7	0.98	nd–118	nd–407	0.79
Mn	9–91.5	35	15–209	219–4981	700

* Similar compositional ranges were indicated by Schwarzinger (2019), and it appears that those data were incorporated into the ranges given by Bindereif *et al.* (2020). Median values are not given for the Madagascar data of Bindereif *et al.* (2020) due to the presence of mixed andradite and andradite-grossular compositions. Abbreviation: nd = not detected.

Figure 32: Trace-element data from 14 point analyses of five samples of Madagascar demantoid (Bindereif *et al.* 2020) show similar trends for Al, Ti and V, with elevated Ti and V when Al is high. Less correlation is shown by Cr, with concentrations that are higher only when Al is elevated.

V and Cr concentrations only occur where the Al concentration is high (Figure 32). Similarly, when the grossular component increases, the REE pattern will change, leading to a depletion in light REEs and an enrichment in moderately heavy REEs, as well as a trend towards a negative Eu anomaly (Bocchio *et al.* 2010).

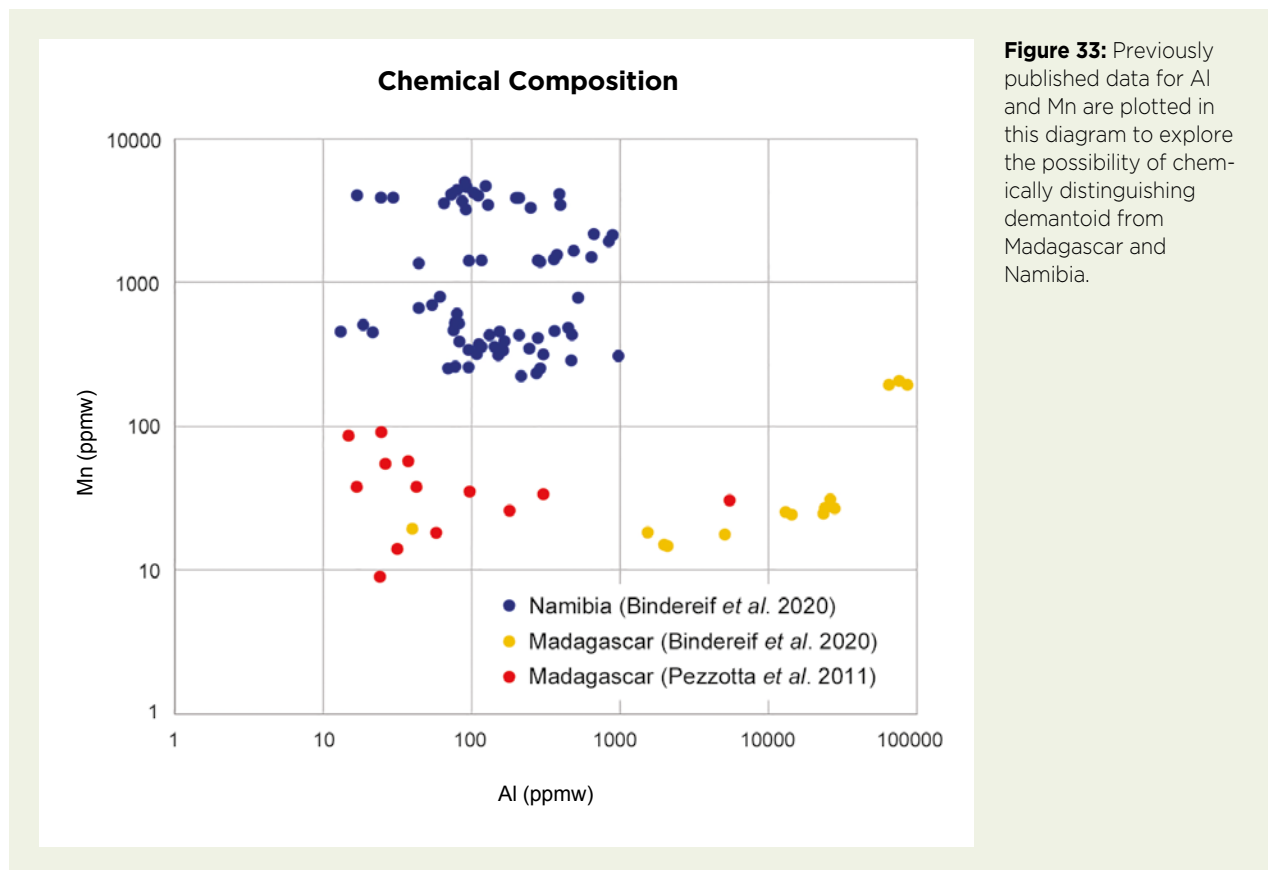From this, it can be concluded: (1) although an enriched Al content could help separate skarn-hosted from serpentinite-hosted demantoid, it cannot be used to confidently separate Malagasy from Namibian stones; and (2) only analyses showing a nearly pure andradite composition should be used for comparing and assessing geographic origin. From the available data (Pezzotta *et al.* 2011; Bindereif *et al.* 2020), plotting Mn vs Al concentrations provides a possible way to distinguish demantoid from Madagascar and Namibia (see Table I and Figure 33). However, more data are needed to test this hypothesis.

CONCLUSION

Detailed characterisation of mineral and fluid inclusions in demantoid from Madagascar showed distinctive features that can be used to determine their geological (skarn) origin. These include diopside clusters (with or without wollastonite, carbonates, quartz and fluorapatite), negative crystals (which are commonly large and empty, but occasionally filled with aqueous liquid and vapour), and partially healed fissures (showing various forms and containing aqueous liquid and vapour, with varying salinities of <20 wt.% NaCl equivalent). When present, native bismuth inclusions appear to be diagnostic for a Madagascar origin; to date they have not been reported in demantoid from any other locality.

Compared with demantoid from serpentinised rocks, stones from skarn-hosted deposits in Madagascar and Namibia show no significant or very low Cr, V and Ti, low Mg and Mn, high REE concentrations, and enriched Al in some samples. A review of available data indicates that only analyses showing a nearly pure andradite composition should be used for assessing geographic origin. For such samples, it appears that a very low Mn content is indicative of a Madagascar origin as compared to material from Namibia.

Chemical Composition

Figure 33: Previously published data for Al and Mn are plotted in this diagram to explore the possibility of chemically distinguishing demantoid from Madagascar and Namibia.

- Namibia (Bindereif *et al.* 2020)
- Madagascar (Bindereif *et al.* 2020)
- Madagascar (Pezzotta *et al.* 2011)

REFERENCES

Adamo, I., Bocchio, R., Diella, V., Pavese, A., Vignola, P., Prosperi, L. & Palanza, V. 2009. Demantoid from Val Malenco, Italy: Review and update. *Gems & Gemology*, **45**(4), 280–287, https://doi.org/10.5741/gems.45.4.280.

Adamo, I., Bocchio, R., Diella, V., Caucia, F. & Schmetzer, K. 2015. Demantoid from Balochistan, Pakistan: Gemmological and mineralogical characterization. *Journal of Gemmology*, **34**(5), 428–433, https://doi.org/10.15506/JoG.2015.34.5.428.

Barrois, O., Giuliani, G., Hafeznia, Y., Zeenabad, H.A., Rakotondrazafy, A.F.M., Ohnenstetter, D., Fallick, A.E., Mathieu, S. *et al.* 2013. Caractéristiques mineralogique et chimique des démantoides de Bagh Borj (Iran) et d'Antetezambato (Madagascar): Consequences geologiques, 2ème partie, études mineralogique et chimique. *Revue de Gemmologie A.F.G.*, No. 183, 10–15.

Bindereif, S., Rüll, F., Schwarzinger, S. & Schwarzinger, C. 2020. Chemometric modeling of trace element data for origin determination of demantoid garnets. *Minerals*, **10**(12), article 1046 (15 pp.) and supplementary table S1 (9 pp.), https://doi.org/10.3390/min10121046.

Bocchio, R., Adamo, I. & Diella, V. 2010. The profile of trace elements, including the REE, in gem-quality green andradite from classic localities. *Canadian Mineralogist*, **48**(5), 1205–1216, https://doi.org/10.3749/canmin.48.5.1205.

Bodnar, R.J. 2003. Introduction to aqueous-electrolyte fluid inclusions. *In*: Samson, I., Anderson, A. & Marshall, D. (eds) *Fluid Inclusions: Analysis and Interpretation*. Mineralogical Association of Canada, Québec, Canada, 81–100.

Buzatu, A. & Buzgar, N. 2010. The Raman study of single-chain silicates. *Analele Ştiinţifice Ale Universităţii "Al. I. Cuza" Iaşi*, **56**(1), 107–125.

Chukanov, N.V. & Vigasina, M.F. 2020. Raman spectra of minerals. *In*: *Vibrational (Infrared and Raman) Spectra of Minerals and Related Compounds*. Springer, Cham, Switzerland, 741–1255, https://doi.org/10.1007/978-3-030-26803-9_4.

Claverie, R., Fontana, M.D., Duričković, I., Bourson, P., Marchetti, M. & Chassot, J.-M. 2010. Optical sensor for characterizing the phase transition in salted solutions. *Sensors*, **10**(4), 3815–3823, https://doi.org/10.3390/s100403815.

Du Toit, G., Mayerson, W., van der Bogert, C., Douman, M., Befi, R., Koivula, J.I. & Kiefert, L. 2006. Demantoid from Iran. *Gems & Gemology*, **42**(3), 131.

Giuliani, G., Pignatelli, I., Fallick, A., Boyce, A., Andriamamonjy, A., Razafindratsimba, S. & Khan, T. 2017. Gem andradite garnet deposits demantoid variety. *InColor*, No. 36, 28–39.

Gomelsky, V. & Bates, R. 2021. Guest John Ferry. The Jewelry District podcast, episode 38, 16 February, https://www.jckonline.com/editorial-article/podcast-jewelry-district-ep-38.

Gübelin, E.J. & Koivula, J.I. 2005. *Photoatlas of Inclusions in Gemstones*, Vol. 2. Opinio Publishers, Basel, Switzerland, 829 pp.

Huang, E., Chen, C.H., Huang, T., Lin, E.H. & Xu, J. 2000. Raman spectroscopic characteristics of Mg-Fe-Ca pyroxenes. *American Mineralogist*, **85**(3–4), 473–479, https://doi.org/10.2138/am-2000-0408.

Koller, F., Niedermayr, G., Pintér, Z. & Szabó, C. 2012. The demantoid garnets of the Green Dragon mine (Tubussi [*sic*], Erongo region, Namibia). *Acta Mineralogica-Petrographica, Abstract Series*, **7**, 72, http://acta.bibl.u-szeged.hu/39436/1/mineralogica_as_007.pdf.

Krzemnicki, M.S. 1999. Diopside needles as inclusions in demantoid garnet from Russia: A Raman microspectrometric study. *Gems & Gemology*, **35**(4), 192–195, https://doi.org/10.5741/gems.35.4.192.

Lewis, Z. 2018. Beyond 'horse tails' in demantoid garnet. *Gems&Jewellery*, **27**(4), 32–35.

Lind, T., Henn, U. & Bank, H. 1998. New occurrence of demantoid in Namibia. *Australian Gemmologist*, **43**(3), 153–160.

Martinez-Uriarte, L., Dubessy, J., Bihannic, I., Boulet, P. & Robert, P. 2014. Reference Raman spectra of $CaCl_2.nH_2O$ solids (n= 0, 2, 4, 6). *11th International GeoRaman Conference*, St Louis, Missouri, USA, 15–19 June, abstract 5069.

Milisenda, C.C. & Hunziker, J. 1999. Demantoid aus Eritrea. *Zeitschrift der Deutschen Gemmologischen Gesellschaft*, **20**, 75–79.

Milisenda, C.C., Henn, U. & Henn, J. 2001. Demantoide aus Pakistan. *Gemmologie: Zeitschrift der Deutschen Gemmologischen Gesellschaft*, **50**(1), 51–56.

Palke, A.C. & Pardieu, V. 2014. Gem News International: Demantoid from Baluchistan Province in Pakistan. *Gems & Gemology*, **50**(4), 302–303.

Pezzotta, F. 2010. Andradite from Antetezambato, north Madagascar. *Mineralogical Record*, **41**(3), 209–229.

Pezzotta, F., Adamo, I. & Diella, V. 2011. Demantoid and topazolite from Antetezambato, northern Madagascar: Review and new data. *Gems & Gemology*, **47**(1), 2–14, https://doi.org/10.5741/gems.47.1.2.

Roedder, E. 1984. *Fluid Inclusions*. Reviews in Mineralogy, **12**, Mineralogical Society of America, Washington DC, USA, vi + 646 pp., https://doi.org/10.1515/9781501508271.

Rondeau, B., Fritsch, E., Mocquet, B. & Lulzac, Y. 2009. Ambanja (Madagascar) – A new source of gem demantoid garnet. *InColor*, No. 11, 22–24.

Rudolph, W.W. & Irmer, G. 2013. Hydration of the calcium(II) ion in an aqueous solution of common anions (ClO_4^-, Cl^-, Br^-, and NO_3^-). *Dalton Transactions*, **42**, 3919–3935, https://doi.org/10.1039/c2dt31718d.

Schwarzinger, C. 2019. Determination of demantoid garnet origin by chemical fingerprinting. *Monatshefte für Chemie - Chemical Monthly*, **150**(5), 907–912, https://doi.org/10.1007/s00706-019-02409-3.

Štubňa, J., Bačík, P., Fridrichová, J., Hanus, R., Illášová, Ľ., Milovská, S., Škoda, R., Vaculovič, T. *et al.* 2019. Gem-quality green Cr-bearing andradite (var. demantoid) from Dobšiná, Slovakia. *Minerals*, **9**(3), article 164 (12 pp.), https://doi.org/10.3390/min9030164.

Sun, Q. 2010. The single donator–single acceptor hydrogen bonding structure in water probed by Raman spectroscopy. *Journal of Chemical Physics*, **132**(5), article 054507 (4 pp.), https://doi.org/10.1063/1.3308496.

Tribaudino, M., Mantovani, L., Bersani, D. & Lottici, P.P. 2012. Raman spectroscopy of $(Ca,Mg)MgSi_2O_6$ clinopyroxenes. *American Mineralogist*, **97**(8–9), 1339–1347, https://doi.org/10.2138/am.2012.4057.

Zepeda, M.A., Picquart, M. & Haro-Poniatowski, E. 2012. Laser induced oxidation effects in bismuth thin films. *MRS Proceedings*, **1477**, 28–33, https://doi.org/10.1557/opl.2012.1720.

The Author

Dr J. C. (Hanco) Zwaan FGA
Netherlands Gem Laboratory,
Naturalis Biodiversity Center,
Darwinweg 2, 2333 CR Leiden,
The Netherlands
Email: hanco.zwaan@naturalis.nl